Research Article Vol. 31, No. 4 / 13 Feb 2023 / Optics Express 6475

Optics EXPRESS

Single-cavity dual-modelocked 2.36-µm laser

AJANTA BARH,[1,2,*] ALEXANDER NUSSBAUM-LAPPING,[1,2] JONAS HEIDRICH,[1] MARCO GAULKE,[1] MATTHIAS GOLLING,[1] CHRISTOPHER R. PHILLIPS,[1] AND URSULA KELLER[1]

[1] *Department of Physics, Institute for Quantum Electronics, ETH Zurich, CH-8093, Switzerland*
[2] *The authors contributed equally to this work*
[*] *ajbarh@phys.ethz.ch*

Abstract: We present the first dual-modelocked femtosecond oscillator operating beyond 2 µm wavelength. This new class of laser is based on a Cr:ZnS gain medium, an InGaSb SESAM for modelocking, and a two-surface reflective device for spatial duplexing of the two modelocked pulse trains (combs). The laser operates at 2.36 µm, and for each comb, we have achieved a FWHM spectral bandwidth of 30 nm, an average power of over 200 mW, and a pulse duration close to 200 fs. The nominal repetition rate is 242 MHz with a sufficiently large repetition rate difference of 4.17 kHz. We also found that the laser is able to produce stable modelocked pulses over a wide range of output powers. This result represents a significant step towards realizing dual-comb applications directly above 2 µm using a single free-running laser.

1. Introduction

Ultrafast laser-based dual-comb sources, consisting of a pair of mutually coherent optical frequency combs (OFCs) with a small difference in their frequency spacing (pulse repetition rate), are currently a major topic of research as they offer fine spectral resolution at a high speed of measurement. Such light sources have diverse applications based on both time and frequency domain measurements, including asynchronous optical sampling [1] or equivalent time sampling [2], laser ranging [3–5], and high-resolution spectroscopy [6–10]. Though most of the ultrafast laser technologies are evolving around near-infrared wavelengths, there is a strong interest for mid-infrared (mid-IR) and short-wave infrared (SWIR) applications [11]. For example, the interesting molecular fingerprint absorption lines can be easily resolved with dual-comb spectroscopy in the spectral range beyond 2 µm, where many important molecules have large and nonoverlapping absorption cross-sections.

The highest power and broad wavelength coverage for OFCs above 2 µm are achieved using nonlinear frequency conversion processes, where dual-comb applications are demonstrated using OPO [7,12] and DFG [8] sources. These schemes rely on long wavelength pump lasers in order to use the well-developed non-oxide nonlinear crystals for efficient and broadband mid-IR light generation [13,14]. Nonetheless, DFG and especially OPO-based schemes are relatively complex and alignment-critical. This complexity can be mitigated by using a direct laser source for dual-comb applications above 2 µm. Quantum cascade lasers (QCLs) [15] and interband cascade lasers (ICLs) [16] are currently the primary industrial sources for mid-IR sensing since they are chip-scale electrically pumped devices. QCLs can provide up to watt-level continuous wave (cw) power [17] and both QCLs and ICLs are used in dual-comb studies [18–20]. But their bandwidth is rather low (<1 THz), and a pulse shaper is required to obtain ultrashort pulses from the chirped output waveform [21]. In contrast, long-wavelength modelocked oscillators offer high peak power pulses suited for driving nonlinear conversion and spectral broadening to the mid-IR, as well as ultralow noise and compatibility with carrier envelope offset stabilization for absolute frequency calibration. This motivates us to establish ultrafast laser-based dual-combs directly above 2 µm.

#481789 https://doi.org/10.1364/OE.481789
Journal © 2023 Received 24 Nov 2022; revised 21 Jan 2023; accepted 21 Jan 2023; published 8 Feb 2023

Optics EXPRESS

Recently, there is a trend in generating the pair of OFCs from a single laser cavity [22,23], where the common-mode noise can be significantly rejected [24,25] and hence, mutual coherence can be established without any active stabilization loop. Such lasers can enable high-precision measurements even in free-running operation [4,26,27]. Most of the progress in this area has been in the near-infrared range [24,28–30]. Extending dual-modelocking to longer wavelengths around 2 µm has been explored using Tm-doped fiber lasers [31–33]. With these lasers, only a few mW of output power is achieved while operating at low repetition rates in the 10's of MHz range. Furthermore, in most cases, these pair of pulse trains correspond to two separate spectral bands, commonly known as dual-wavelength modelocking. Such a laser requires an additional amplification stage to boost the power and a nonlinear spectral broadening stage to achieve overlapped spectra, which then makes it suitable for coherent dual-comb applications [33].

Here we present a single-cavity dual-modelocking of a Cr:ZnS solid-state laser operating at 2.36 µm and modelocked with an InGaSb quantum well SESAM [34,35]. The laser produces two modelocked pulse trains (combs), each with more than 200 mW average power and pulse duration close to 200 fs. The fundamental repetition rate is 242 MHz with a repetition rate difference of 4.17 kHz. Though 2.4-µm Cr:ZnS(e)-based comb sources [36] and two separate laser-based dual-comb applications have been presented [37,38], single-cavity dual-modelocking has never been demonstrated using this type of laser. Thus, our results hold a set of novelties, which includes first dual-modelocking (i) above 2 µm wavelength and (ii) of a Cr:ZnS laser. Furthermore, (iii) the laser produces the highest power and the shortest pulse at two comb modes directly from a single oscillator in the 2-µm range.

Optically pumped Cr:ZnS(e) solid-state lasers are gaining wider interest in recent years owing to their reliable fabrication quality, broad spectral coverage (2–3 µm), and other properties suitable for high-power and short pulse generation [34,39–42]. Though the widely used Kerr-lens modelocking is ideal for few-cycle pulse generation [40,42] and used in applications [43,44], SESAM modelocking offers robust, low-noise, and self-starting operation. Our recent effort on novel InGaSb material-based SESAMs has enabled self-starting Cr:ZnS lasers delivering stable high-power [34] and high-repetition rate [45] femtosecond pulses. In the end, this allowed us to establish stable dual-modelocking of the laser, as reported herein.

2. Dual-modelocking of Cr:ZnS laser

2.1. Pump configuration

The dual-comb SESAM-modelocked Cr:ZnS laser presented here is pumped by an Er-doped fiber laser (NKT Photonics, Koheras BoostiK E15 PM FM), which in the future can also be extended to diode-pumping [46]. A 1550-nm Er-doped linearly polarized single mode fiber laser providing up to 10 W of cw power is used for pumping a 3.8-mm long polycrystalline Cr:ZnS gain element with a specified doping concentration of $9 \times 10^{18}/\text{cm}^3$ (IPG Photonics). The power is (equally) divided over two arms and guided through an optical telescope arrangement for beam scaling. In the end, the two beams are focused into the gain element using a 50-mm focal length lens, where the spot size of each beam is ~ 57 µm in radius with a spatial separation of ~ 1.4 mm. These values are adjusted as per laser cavity design (Section 2.2).

The Cr:ZnS sample has transverse dimensions of 2.2 mm (h) × 3.2 mm (w) and is Brewster-cut along the w-side. The sample is oriented in a way to obtain the Brewster condition for horizontal polarization and to establish the beam path on a horizontal plane. With the spatial duplexing design (more details in Section 2.2) the two beams are slightly displaced in the vertical (h) direction at the gain element (to avoid any cross-talk). This ensures that both beams are focused near the center of the sample and are not clipped due to the angular incidence in the w-direction. During optimization of their spot size and position, we further observed that the pump absorption is not uniform across the h-direction. We have measured the small signal transmission of 1550-nm

Optics EXPRESS

pump with 64 mW power by translating the gain element in the *h*-direction. The result is plotted in Fig. 1(a). The transmission drops significantly towards both edges, which can be explained by the fact that Cr is diffusion doped into the ZnS sample through the sides. Even so, this actually favors our dual-pump configuration, where the two beams are separated nearly symmetrically from the center and a higher pump absorption is obtained.

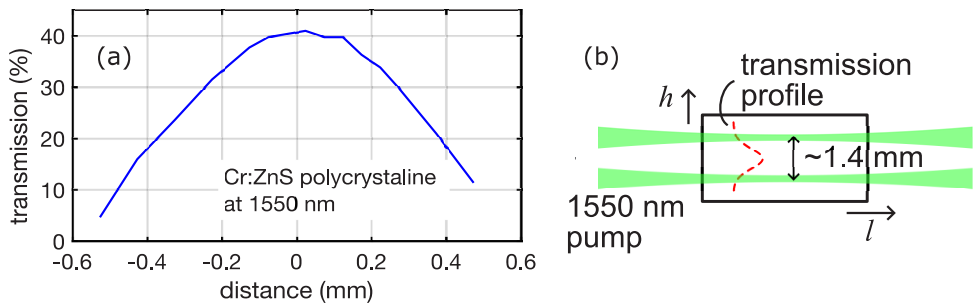

Fig. 1. (a) Transmission profile of 1550-nm pump through the Cr:ZnS gain element along the vertical (h) dimension, which decreases nearly symmetrically from the center (distance = 0 mm) towards the edges. (b) Schematic side-view of the gain element showing the two pump positions in the *h*-direction, while propagating along the *l*-direction. A schematic transmission profile (red dashed) is indicated as well.

2.2. Laser cavity configuration

A standard X-folded laser cavity is developed (Fig. 2), where the Cr:ZnS is placed in the middle of the stability zone and temperature stabilized to 16 °C. One arm of this X-folded cavity uses a SESAM as an end mirror, which is mounted on a copper block and temperature stabilized to 22 °C. The SESAM parameters are described in [34,45]. The other arm is ended with a flat output coupler (OC) of 3% average transmission over 2.2–2.6 µm. The input coupling mirror transmits > 93% of the pump power. All the mirrors and the OC have low and nearly flat group delay dispersion (GDD), however, are not optimized for any higher order dispersion. All of the mirrors have the same coating. We placed an uncoated 5-mm long YAG window (which has negative GDD at this wavelength) at Brewster's angle inside the cavity to adjust the total cavity GDD to a value suitable for fundamental soliton modelocking [47]. The GDD and reflectivity of cavity elements are described in more details in [34]. The astigmatism introduced by the curved mirrors, Cr:ZnS and YAG is minimized by choosing incident angles on the turning mirrors of ~ 5°. The laser is mounted on an optical breadboard and operated in a standard laboratory environment.

The cavity is designed for two modelocked pulse trains (combs) displaced spatially (vertically) by using a two-surface device, with two separate angles on its surface (apex angle ~ 178.5°, inset in Fig. 2(a)). The device is similar to a Fresnel biprism that has been used for dual-comb modelocking at 1 µm wavelength [28], but in our case, it is made of two separate optical substrates. The cavity design was chosen to obtain appropriate mode sizes on the active elements and to allow for reasonable beam separation on the highly-reflective coated duplexing device when placed in the proper position. This means that two equally efficient combs with the same polarization (horizontal) are created with slightly different repetition rates (intracavity optical path length). Both combs follow a quasi-common path and share all of the same cavity elements. The spot size variation of one comb inside the cavity is plotted in Fig. 2(b). The estimated laser mode size on the gain element is ~ 59 µm in radius, which matches well with the pump spot size of ~ 57 µm. With an estimated spot size on the SESAM of ~148 µm, the average fluence (i.e., the half peak fluence for a Gaussian beam) is ~ 49 µJ/cm^2 at the highest stable modelocked power

Optics EXPRESS

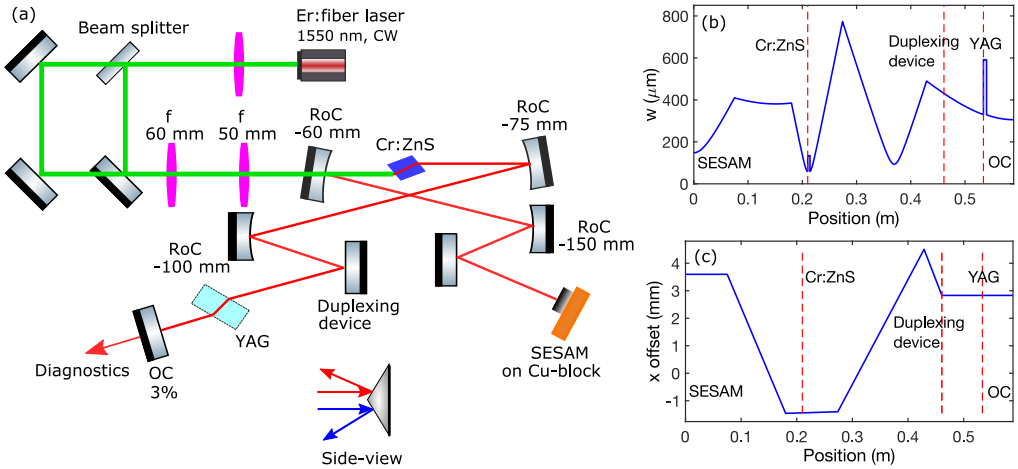

Fig. 2. (a) Schematic top-view of the dual-comb soliton modelocked Cr:ZnS laser cavity using the SESAM to start and stabilize passive modelocking. The two beam paths are vertically displaced, where the gain element and YAG window are placed at (horizontal) Brewster's angle for lowest loss. The pump beam is split and recombined with a vertical displacement. Thus, only one beam path is visible from this view. The turning mirrors and duplexing device are coated for high reflection over 2.1–3.0 µm. The radius of curvature (RoC) is indicated for each curved mirror. The Cr:ZnS, duplexing device, and SESAM are mounted on a translational stage for fine positioning. The inset shows a side-view of the duplexing device with two beams indicated in different colors. The arrows indicate the path taken by the intracavity beams returning from the OC. A cavity simulation shows the variation of (b) laser mode size (radius) in Brewster plane, and (c) vertical offset of one mode from the other. The red vertical lines indicate the position of Cr:ZnS, duplexing device, and YAG, whereas the SESAM and the OC are positioned at two ends of the cavity.

for each comb. The combs are well separated both in the gain element (~ 1.4 mm) and on the SESAM (~ 3.5 mm), ensuring minimum cross-talk between them at the active elements. The calculated vertical offset between the two combs is plotted in Fig. 2(c), which also indicates that the beams are well separated at the output (~ 3 mm at the OC). With this design, we obtain stable simultaneous passive modelocking for both the combs.

3. Modelocking characterization

We characterize the laser by measuring modelocking diagnostics, which consists of an optical spectrum analyzer (OSA), second harmonic generation (SHG)-based intensity autocorrelator, microwave spectrum analyzer (MSA), and a home-built SHG setup using a 5-mm long periodically poled lithium niobate crystal. The pulses experience -3000 fs^2 of GDD before reaching the autocorrelator. With the SESAM in place, simultaneous self-starting soliton modelocking [47] is established for the dual-combs with very similar properties. Stable modelocking is established for a wide range of output laser power as shown in Fig. 3(a). Close to transform-limited pulse duration is achieved over this entire range (cross in Fig. 3(a)). The decrease in pulse duration with increasing power is a strong indication of a soliton modelocking mechanism for the pulse formation, for which the SESAM starts and stabilizes the soliton formation. The saturation behavior in the pulse duration measurements can be attributed to thermal lensing in the cavity and to a power-dependent red shift of the center wavelength (~11 nm from minimum to maximum power). Nevertheless, we obtain up to 250 mW (200 mW) for comb 1 (comb 2) with a pulse duration of 207 fs (187 fs). At this power level, the estimated optical-to-optical efficiency with

Optics EXPRESS

respect to absorbed pump power is >10% and an excellent transverse beam quality is achieved. A full parameter set is displayed in Table 1. Further increase in pump power resulted in instability of the modelocked states.

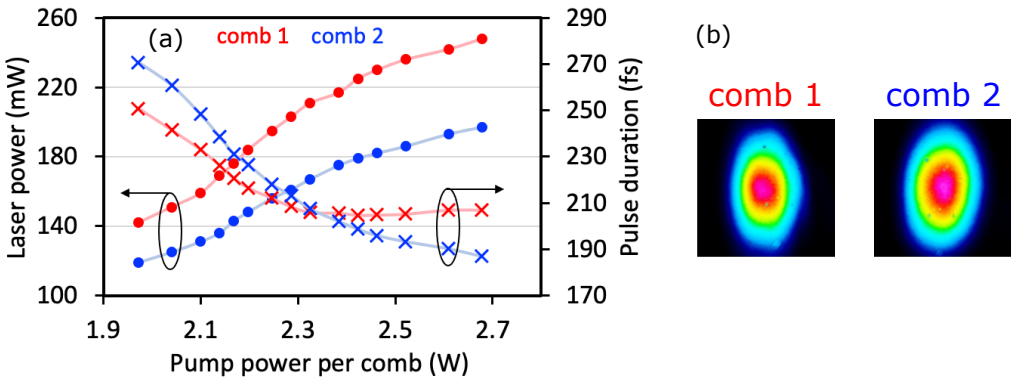

Fig. 3. Modelocking performance. (a) Measured laser output power (solid circle) and pulse duration (cross) for different pump power per comb. Red: comb 1. Blue: comb 2. (b) Measured beam profile for the two lasing modes.

Table 1. Laser Parameters at Highest Power Stable Modelocked State

Parameters	Power (mW)	Center wavelength (nm)	Bandwidth (nm)	Pulse duration (fs)	Peak power (kW)	f_{rep} (MHz)	Δf_{rep} (kHz)
comb 1	250	2363	29	207	4.4	242	4.17
comb 2	200	2357	32	187	3.9		

The measured autocorrelator trace is shown in Fig. 4(a)-(b), and the corresponding optical spectrum in Fig. 4(c), with a full-width at half-maximum (FWHM) bandwidth of 29 nm (32 nm). These spectra are fully overlapped, which is highly beneficial for dual-comb spectroscopic applications. Because of the lack of high-speed photodetectors at 2.4 µm, a direct measurement of the pulse repetition rate was not possible. Instead, we have used an external SHG setup to translate the laser output to a more accessible near-infrared range which is detected using a fast (45 GHz) InGaAs detector connected to an MSA with a bandwidth of 13.2 GHz. Both combs show fundamental modelocking at a repetition rate f_{rep} of ~ 242 MHz with an offset (Δf_{rep}) of 4.17 kHz. With our single SHG setup, we could not measure both repetition rates simultaneously. Instead, we measured them in sequence (by using a beam combiner and a flip mirror in the beam diagnostics path) and confirmed their stability. The two measured radio frequency peaks are combined and plotted in Fig. 4(d), clearly indicating the offset and a high signal-to-noise ratio for both measurements. The offset repetition rate can be slightly adjusted by translating the duplexing device in vertical direction, since this introduces variation in relative path length for the two modes. However, it is limited by the spatial mode separation on it and the clipping of a mode at its apex angle position.

Optics EXPRESS

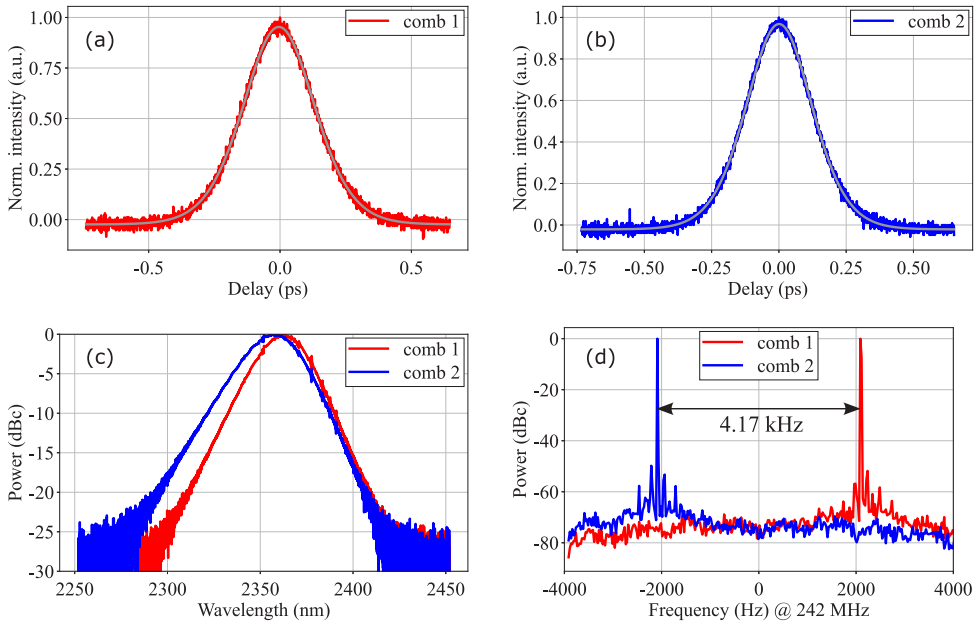

Fig. 4. Measured dual-comb Cr:ZnS laser performance at highest average output power. Intensity autocorrelation trace with sech^2 fit for (a) comb 1 and (b) comb 2. (c) Optical spectrum of comb 1 (red) and comb 2 (blue), showing a fully overlapped spectrum. (d) Radio frequency trace centered at 242 MHz measured with a resolution bandwidth of 3 Hz. The Δf_{rep} of 4.17 kHz is indicated by an arrow.

4. Discussion

This dual-modelocked laser is operated in the middle of its stability zone and is self-starting. To operate both combs simultaneously it is necessary to overlap the two pump spots with the two cavity modes in the gain medium. For that, we have adjusted the pump beam path as required. The beams are well separated on the SESAM, ensuring no coupling between the two similar comb modes as discussed previously in more detail [30]. This similar performance also indicates that the SESAM parameters are uniform across the device. Furthermore, even at highest power operation, we did not observe any noticeable damage on it. The transverse (vertical) dimension of our gain element is only 2.2 mm and the clear aperture is even lower. So, we limited our beam separation to ~ 1.4 mm inside it. However, our results indicate that this separation is good enough to avoid any cross-talk between the modes, and we could use a higher gain section of the gain element for the laser operation (as discussed in Section 2.1). Due to the polycrystalline nature and Brewster angle cut, the gain element might exhibit non-symmetric and non-uniform heat distribution, which causes misalignment in the cavity while ramping up the power and eventually shows a saturation behavior (Fig. 3(a)). The small ellipticity in the laser beam profiles is due to residual astigmatism inside the cavity, which can be eliminated by further design optimization. The two-surface reflective device allows for robust spatial multiplexing, where both combs share all of the same cavity elements. This is useful for common noise suppression, a highly desired property for dual-comb applications. Unlike dual-wavelength modelocking, our laser produces a well overlapped and broad optical spectrum, highly suited for dual-comb spectroscopy.

Optics EXPRESS

5. Conclusion

In conclusion, we demonstrate the first dual-modelocked laser beyond 2 µm operating wavelength. We have achieved this milestone by using a Cr:ZnS solid-state laser with passive soliton modelocking using an in-house grown InGaSb quantum well SESAM, and a reflective two-surface device for spatial duplexing of the two cavity modes. The laser generates two self-starting modelocked pulse trains at a center wavelength of ~ 2.36 µm with an average output power up to 250 mW (200 mW) and pulse duration of 207 fs (187 fs) at a nominal repetition rate of 242 MHz. We obtained a sufficiently large repetition rate difference of 4.17 kHz and a wide optical spectrum of ~ 30 nm for both combs. Further power scaling can be done by using a higher output coupling rate, which will also improve the heat management of the gain element for better performance. We used a standard X-fold cavity with a small footprint maintaining low intracavity losses and robust operation. These parameters are important for rapid and sensitive measurements. Thus, our result paves the way towards single laser-based dual-comb applications directly in the important 2–3 µm spectral range, suitable for rapid pump-probe measurements and high-resolution molecular spectroscopy.

Funding. European Research Council (ERC advanced grant 787097 ONE-MIX); Schweizerischer Nationalfonds zur Förderung der Wissenschaftlichen Forschung (BRIDGE Discovery 40B2-0_180933).

Acknowledgments. We thank FIRST cleanroom facility of ETH Zurich for the SESAM growth, and Dr. V. Wittwer of U. of. Neuchatel for the coating on output coupler.

Disclosures. The authors declare no conflicts of interest.

Data availability. Data underlying the results presented in this paper are not publicly available at this time but may be obtained from the authors upon reasonable request.

References

1. P. A. Elzinga, R. J. Kneisler, F. E. Lytle, Y. Jiang, G. B. King, and N. M. Laurendeau, "Pump/probe method for fast analysis of visible spectral signatures utilizing asynchronous optical sampling," Appl. Opt. **26**(19), 4303–4309 (1987).
2. K. J. Weingarten, M. J. W. Rodwell, H. K. Heinrich, B. H. Kolner, and D. M. Bloom, "Direct electro-optic sampling of GaAs integrated circuits," Electron. Lett. **21**(17), 765–766 (1985).
3. Z. Zhu and G. Wu, "Dual-Comb Ranging," Engineering **4**(6), 772–778 (2018).
4. S. L. Camenzind, J. F. Fricke, J. Kellner, B. Willenberg, J. Pupeikis, C. R. Phillips, and U. Keller, "Dynamic and precise long-distance ranging using a free-running dual-comb laser," Opt. Express **30**(21), 37245–37260 (2022).
5. B. Martin, B. Martin, P. Feneyrou, D. Dolfi, and A. Martin, "Performance and limitations of dual-comb based ranging systems," Opt. Express **30**(3), 4005–4016 (2022).
6. I. Coddington, N. Newbury, and W. Swann, "Dual-comb spectroscopy," Optica **3**(4), 414–426 (2016).
7. O. Kara, L. Maidment, T. Gardiner, P. G. Schunemann, and D. T. Reid, "Dual-comb spectroscopy in the spectral fingerprint region using OPGaP optical parametric oscillators," Opt. Express **25**(26), 32713–32721 (2017).
8. G. Ycas, F. R. Giorgetta, E. Baumann, I. Coddington, D. Herman, S. A. Diddams, and N. R. Newbury, "High-coherence mid-infrared dual-comb spectroscopy spanning 2.6 to 5.2 µm," Nat. Photonics **12**(4), 202–208 (2018).
9. M. Yu, Y. Okawachi, A. G. Griffith, N. Picqué, M. Lipson, and A. L. Gaeta, "Silicon-chip-based mid-infrared dual-comb spectroscopy," Nat. Commun. **9**(1), 1869 (2018).
10. M. A. Abbas, Q. Pan, J. Mandon, S. M. Cristescu, F. J. M. Harren, and A. Khodabakhsh, "Time-resolved mid-infrared dual-comb spectroscopy," Sci. Rep. **9**(1), 17247 (2019).
11. A. Schliesser, N. Picqué, and T. W. Hänsch, "Mid-infrared frequency combs," Nat. Photonics **6**(7), 440–449 (2012).
12. A. V. Muraviev, V. O. Smolski, Z. E. Loparo, and K. L. Vodopyanov, "Massively parallel sensing of trace molecules and their isotopologues with broadband subharmonic mid-infrared frequency combs," Nat. Photonics **12**(4), 209–214 (2018).
13. V. Smolski, S. Vasilyev, I. Moskalev, M. Mirov, Q. Ru, A. Muraviev, P. Schunemann, S. Mirov, V. Gapontsev, and K. Vodopyanov, "Half-Watt average power femtosecond source spanning 3–8 µm based on subharmonic generation in GaAs," Appl. Phys. B **124**(6), 101 (2018).
14. C. Gaida, M. Gebhardt, T. Heuermann, F. Stutzki, C. Jauregui, J. Antonio-Lopez, A. Schülzgen, R. Amezcua-Correa, A. Tünnermann, I. Pupeza, and J. Limpert, "Watt-scale super-octave mid-infrared intrapulse difference frequency generation," Light: Sci. Appl. **7**(1), 94 (2018).
15. J. Faist, F. Capasso, D. L. Sivco, C. Sirtori, A. L. Hutchinson, and A. Y. Cho, "Quantum Cascade Laser," Science **264**(5158), 553–556 (1994).
16. J. Hillbrand, M. Beiser, A. M. Andrews, H. Detz, R. Weih, A. Schade, S. Höfling, G. Strasser, and B. Schwarz, "Picosecond pulses from a mid-infrared interband cascade laser," Optica **6**(10), 1334–1337 (2019).

Optics EXPRESS

17. D. Botez, J. D. Kirch, C. Boyle, K. M. Oresick, C. Sigler, H. Kim, B. B. Knipfer, J. H. Ryu, D. Lindberg, T. Earles, L. J. Mawst, and Y. V. Flores, "High-efficiency, high-power mid-infrared quantum cascade lasers [Invited]," Opt. Mater. Express **8**(5), 1378–1398 (2018).
18. G. Villares, A. Hugi, S. Blaser, and J. Faist, "Dual-comb spectroscopy based on quantum-cascade-laser frequency combs," Nat. Commun. **5**(1), 5192 (2014).
19. M. Gianella, A. Nataraj, B. Tuzson, P. Jouy, F. Kapsalidis, M. Beck, M. Mangold, A. Hugi, J. Faist, and L. Emmenegger, "High-resolution and gapless dual comb spectroscopy with current-tuned quantum cascade lasers," Opt. Express **28**(5), 6197–6208 (2020).
20. L. A. Sterczewski, J. Westberg, M. Bagheri, C. Frez, I. Vurgaftman, C. L. Canedy, W. W. Bewley, C. D. Merritt, C. S. Kim, M. Kim, J. R. Meyer, and G. Wysocki, "Mid-infrared dual-comb spectroscopy with interband cascade lasers," Opt. Lett. **44**(8), 2113–2116 (2019).
21. P. Täschler, M. Bertrand, B. Schneider, M. Singleton, P. Jouy, F. Kapsalidis, M. Beck, and J. Faist, "Femtosecond pulses from a mid-infrared quantum cascade laser," Nat. Photonics **15**(12), 919–924 (2021).
22. S. M. Link, A. Klenner, M. Mangold, C. A. Zaugg, M. Golling, B. W. Tilma, and U. Keller, "Dual-comb modelocked laser," Opt. Express **23**(5), 5521–5531 (2015).
23. R. Liao, H. Tian, W. Liu, R. Li, Y. Song, and M. Hu, "Dual-comb generation from a single laser source: principles and spectroscopic applications towards mid-IR—A review," J. Phys. Photonics **2**(4), 042006 (2020).
24. Y. Nakajima, Y. Hata, and K. Minoshima, "High-coherence ultra-broadband bidirectional dual-comb fiber laser," Opt. Express **27**(5), 5931–5944 (2019).
25. C. R. Phillips, B. Willenberg, A. Nussbaum-Lapping, F. Callegari, S. L. Camenzind, J. Pupeikis, and U. Keller, "Coherently averaged dual-comb spectroscopy with a low-noise and high-power free-running gigahertz dual-comb laser," *Opt. Express* in press (2023).
26. S. M. Link, D. J. H. C. Maas, D. Waldburger, and U. Keller, "Dual-comb spectroscopy of water vapor with a free-running semiconductor disk laser," Science **356**(6343), 1164–1168 (2017).
27. X. Zhao, G. Hu, B. Zhao, C. Li, Y. Pan, Y. Liu, T. Yasui, and Z. Zheng, "Picometer-resolution dual-comb spectroscopy with a free-running fiber laser," Opt. Express **24**(19), 21833–21845 (2016).
28. J. Pupeikis, B. Willenberg, S. L. Camenzind, A. Benayad, P. Camy, C. R. Phillips, and U. Keller, "Spatially multiplexed single-cavity dual-comb laser," Optica **9**(7), 713–716 (2022).
29. K. Fritsch, T. Hofer, J. Brons, M. Iandulskii, K. F. Mak, Z. Chen, N. Picqué, and O. Pronin, "Dual-comb thin-disk oscillator," Nat. Commun. **13**(1), 2584 (2022).
30. S. M. Link, A. Klenner, and U. Keller, "Dual-comb modelocked lasers: semiconductor saturable absorber mirror decouples noise stabilization," Opt. Express **24**(3), 1889–1902 (2016).
31. Y. Wang, J. Li, B. Zhai, Y. Hu, K. Mo, R. Lu, and Y. Liu, "Tunable and switchable dual-wavelength mode-locked Tm3+-doped fiber laser based on a fiber taper," Opt. Express **24**(14), 15299–15306 (2016).
32. H. Jiang, Y. Wang, S. Y. Set, and S. Yamashita, "Bidirectional Mode-locked Soliton Fiber Laser in 2μm Using CNT Saturable Absorber," in *Laser Congress 2017 (ASSL, LAC) (2017), Paper JM5A.21* (Optical Society of America, 2017), p. JM5A.21.
33. R. Liao, Y. Song, W. Liu, H. Shi, L. Chai, and M. Hu, "Dual-comb spectroscopy with a single free-running thulium-doped fiber laser," Opt. Express **26**(8), 11046–11054 (2018).
34. A. Barh, J. Heidrich, B. O. Alaydin, M. Gaulke, M. Golling, C. R. Phillips, and U. Keller, "Watt-level and sub-100-fs self-starting mode-locked 2.4-μm Cr:ZnS oscillator enabled by GaSb-SESAMs," Opt. Express **29**(4), 5934–5946 (2021).
35. B. Ö. Alaydin, M. Gaulke, J. Heidrich, M. Golling, A. Barh, and U. Keller, "Bandgap engineering, monolithic growth, and operation parameters of GaSb-based SESAMs in the 2-2.4 μm range," Opt. Mater. Express **12**(6), 2382–2394 (2022).
36. S. Vasilyev, V. Smolski, J. Peppers, I. Moskalev, M. Mirov, Y. Barnakov, S. Mirov, and V. Gapontsev, "Middle-IR frequency comb based on Cr:ZnS laser," Opt. Express **27**(24), 35079 (2019).
37. B. Bernhardt, E. Sorokin, P. Jacquet, R. Thon, T. Becker, I. T. Sorokina, N. Picqué, and T. W. Hänsch, "Mid-infrared dual-comb spectroscopy with 2.4 μm Cr2+:ZnSe femtosecond lasers," Appl. Phys. B **100**(1), 3–8 (2010).
38. S. Vasilyev, A. Muraviev, D. Konnov, M. Mirov, V. Smoslki, I. Moskalev, S. Mirov, and K. Vodopyanov, "Video-rate broadband longwave IR dual-comb spectroscopy with 240,000 comb-mode resolved data points," (2022).
39. S. B. Mirov, I. S. Moskalev, S. Vasilyev, V. Smolski, V. V. Fedorov, D. Martyshkin, J. Peppers, M. Mirov, A. Dergachev, and V. Gapontsev, "Frontiers of Mid-IR Lasers Based on Transition Metal Doped Chalcogenides," IEEE J. Select. Topics Quantum Electron. **24**(5), 1–29 (2018).
40. S. Vasilyev, I. S. Moskalev, V. O. Smolski, J. M. Peppers, M. Mirov, A. V. Muraviev, K. Zawilski, P. G. Schunemann, S. B. Mirov, K. L. Vodopyanov, and V. P. Gapontsev, "Super-octave longwave mid-infrared coherent transients produced by optical rectification of few-cycle 25-μm pulses," Optica **6**(1), 111–114 (2019).
41. S. Vasilyev, I. Moskalev, M. Mirov, S. Mirov, and V. Gapontsev, "Multi-Watt mid-IR femtosecond polycrystalline Cr^2+:ZnS and Cr^2+:ZnSe laser amplifiers with the spectrum spanning 20–26 μm," Opt. Express **24**(2), 1616–1623 (2016).
42. N. Nagl, S. Gröbmeyer, V. Pervak, F. Krausz, O. Pronin, and K. F. Mak, "Directly diode-pumped, Kerr-lens mode-locked, few-cycle Cr:ZnSe oscillator," Opt. Express **27**(17), 24445–24454 (2019).

Optics EXPRESS

43. V. E. Leshchenko, B. K. Talbert, Y. H. Lai, S. Li, Y. Tang, S. J. Hageman, G. Smith, P. Agostini, L. F. DiMauro, and C. I. Blaga, "High-power few-cycle Cr:ZnSe mid-infrared source for attosecond soft x-ray physics," Optica **7**(8), 981–988 (2020).
44. P. Steinleitner, N. Nagl, M. Kowalczyk, J. Zhang, V. Pervak, C. Hofer, A. Hudzikowski, J. Sotor, A. Weigel, F. Krausz, and K. F. Mak, "Single-cycle infrared waveform control," Nat. Photonics **16**(7), 512–518 (2022).
45. A. Barh, B. Ö. Alaydin, B. Ö. Alaydin, J. Heidrich, M. Gaulke, M. Golling, C. R. Phillips, and U. Keller, "High-power low-noise 2-GHz femtosecond laser oscillator at 2.4 µm," Opt. Express **30**(4), 5019–5025 (2022).
46. J. Heidrich, A. Barh, S. L. Camenzind, B. Willenberg, M. Gaulke, M. Golling, C. R. Phillips, and U. Keller, "Low-Noise Femtosecond SESAM Modelocked Diode-Pumped Cr:ZnS Oscillator," IEEE J. Quantum Electron. in press (2023).
47. F. X. Kärtner, I. D. Jung, and U. Keller, "Soliton mode-locking with saturable absorbers," IEEE J. Sel. Top. Quantum Electron. **2**(3), 540–556 (1996).